Science Advances MAAAS

Manuscript Template

Planar 2D Wireframe DNA Origami

Xiao Wang 1† , Shanshan Li 2,3† , Hyungmin Jun 1,4† , Torsten John 1 , Kaiming Zhang 2,3 , Hannah Fowler 5 , Jonathan P.K. Doye 5 , Wah Chiu 2,6* , Mark Bathe 1*

¹Department of Biological Engineering, Massachusetts Institute of Technology, Cambridge, MA 02139, United States

²Department of Bioengineering, James H. Clark Center, Stanford University, Stanford, CA 94305, United States

³MOE Key Laboratory for Cellular Dynamics, Hefei National Laboratory for Physical Sciences at the Microscale and School of Life Sciences, University of Science and Technology of China, Hefei, Anhui 230027, China

⁴Division of Mechanical System Engineering, Jeonbuk National University, Jeonju-si, Jeollabuk-do 54896, Republic of Korea

⁵Physical and Theoretical Chemistry Laboratory, Department of Chemistry, University of Oxford, Oxford, UK.

⁶Cryo-EM and Bioimaging Division, Stanford Synchrotron Radiation Lightsource, SLAC National Accelerator Laboratory, Stanford University, Menlo Park, CA 94025, USA

†These authors contributed equally to this work

*Corresponding Authors: wahc@stanford.edu; mark.bathe@mit.edu

Abstract

2D DNA origami is widely used for applications ranging from excitonics to single-molecule biophysics. Conventional, single-layer 2D DNA origami exhibits flexibility and curvature in solution, however, that may limit its suitability as a 2D structural template. In contrast, 2D wireframe DNA origami rendered with six-helix bundle edges offers local control over duplex orientations with enhanced in-plane rigidity. Here, we investigate the 3D structure of these assemblies using cryogenic electron microscopy (cryo-EM). 3D reconstructions reveal a high degree of planarity and homogeneity in solution for polygonal objects with and without internal mesh, enabling 10 Å resolution for a triangle. Coarse-grained simulations were in agreement with cryo-EM data, offering molecular structural insight into this new class of 2D DNA origami. Our results suggest these assemblies may be valuable for 2D materials applications and geometries that require high structural fidelity together with local control over duplex orientations, rather than parallel duplex assembly.

Introduction

DNA origami was invented in 2006 by Paul Rothemund¹ by rendering in DNA solid 2D geometries including squares, triangles, stars, and a smiley face. In this first implementation, rectilinear, parallel DNA duplexes were interconnected with crossovers of anti-parallel DNA strands consisting

1 2

of a long scaffold strand from the M13 phage genome hybridized to hundreds of shorter, synthetic staple strands. This rectilinear or bricklike fabrication strategy is powerful because it offers straightforward scaffold strand routing and staple sequence design manually or using simple Computer-Aided Design tools², rendering the technique broadly accessible to non-experts. However, because these 2D origami objects are visualized nearly exclusively on 2D surfaces using Atomic Force Microscopy (AFM) or Transmission Electron Microscopy, objects typically appear flat despite their significant curvature, bend, or twist in 3D solution³⁻⁵. Although 3D structure prediction tools such as CanDo⁶ have been used to reduce out-of-plane deformations⁷⁻⁹, experimental validation of planarity has remained elusive, together with general design rules to attain and maintain planarity for arbitrary 2D geometries. While there have been several attempts to both study and control the planarity of 2D DNA origami rendered with single-layer parallel duplexes in recent years ^{10, 11}, resolving the 3D structure of these assemblies in solution has remained elusive, likely due to their significant flexibility and heterogeneity in solution, corroborated by solution scattering data¹⁰ and AFM¹¹. One exception is a recent 3D cryo-EM study that revealed significant flexibility and curvature of a rectangular origami rendered with single-layer duplexes organized in parallel, as originally implemented by Rothemund¹, whereas the 3D structures of rigid and largely homogeneous multilayer brick-like origami were reconstructed to nucleotide-resolution in the same report 12 .

While experimentally elusive to realize and validate, planarity of 2D origami is of paramount importance to numerous applications that seek to organize secondary materials with nanometer-scale precision¹³⁻¹⁴, including fundamental studies of light-harvesting and excitonics¹⁵⁻¹⁸, single-molecule¹⁹⁻²¹ and super resolution imaging^{19,22}, molecular biophysics²³, photonics²⁴, cellular biophysics²⁵⁻²⁸, and surface-based patterning and lithography^{29,30}. Multilayer honeycomb³¹ and square lattice³² bricklike origami designs offer alternatives to fabricating monolayer 2D origami, but they achieve planarity while reducing the overall lateral dimension of objects that can be rendered due to the increased length of scaffold required; they may require careful sequence design with iterative feedback from structural simulations and experiment to reduce or eliminate intrinsic twist^{6,8,9,32}; and they are largely limited geometrically to rendering rectilinear geometries that consist of parallel duplexes throughout the object, with³³ or without curvature^{1,34}. Attaching 2D monolayer origami to surfaces using high affinity ligand-receptor pairs may be used to partially flatten objects, although experimental validation is again challenging due to the perturbative nature of AFM and the low contrast of TEM, and numerous applications are not amenable to this biochemical immobilization strategy.

As an alternative to rectilinear, bricklike origami, 2D wireframe DNA origami has recently emerged as an alternative for positioning secondary materials in 2D with nanometer-scale precision and local orientational control over duplex axes^{35,36}. Compared with conventional, rectilinear bricklike origami, wireframe geometries can render polyhedral geometries that are not accessible to rectilinear duplex assemblies^{35,36}; they reduce overall scaffold length required to render 2D objects of a given lateral dimension due to their open, meshlike structure that minimizes the use of DNA; and they also offer local orientational control over duplex orientations that may be required for some applications, such as organizing chromophores to control molecular excitonics³⁷⁻³⁹ and photonics³⁰.

The fully automated sequence design tool METIS offers in principle the ability to render planar 2D wireframe objects using multilayer, 6HB edges, although to date experimental characterization has been limited to 2D imaging that suffers similarly from potential artifacts from 2D solid support³⁵. Here, we report results of 3D cryo-EM to resolve the first examples of planar 2D DNA origami structures rendered using 6HB wireframe designs up to 80 nm in lateral dimensions. To test the

breadth and diversity of 2D objects that can be fabricated we explore two distinct categories of wireframe objects, which are polygonal with and without internal structure. And to establish the sizes of objects that can be rendered in this manner we vary lateral edge lengths from 42 bp to 210 bp. 3D reconstruction demonstrates homogeneous, planar objects result from our approach, with resolutions of 10-18 Å that suggest minimal structural deviation from planarity up to an ~80 nm lateral dimension. This new class of planar DNA origami is rendered from the top down using the fully automatic sequence algorithm METIS³⁵ implemented in the Graphical User Interface ATHENA⁴⁰, rendering it broadly useful for 2D nanoscale materials design and patterning.

Results

Computer-aided design of 2D origami

6HB edge-based 2D wireframe DNA origami structures were rendered using METIS³³ within ATHENA⁴⁰ (Fig. 1, Fig. S1). To investigate the planarity of origami objects, diverse target planar geometries were chosen including hexagons, pentagons, and triangles that are symmetric versus asymmetric. To also evaluate the effects of an internal mesh on planarity, we rendered hexagons and pentagons both with and without internal wireframe support (Table S1). Finally, pentagons with different edge lengths were generated as described previously⁴⁰ to explore the impact of lateral dimensions on the planarity attained.

Planarity of 2D wireframe origami

- The METIS algorithm leverages the 6HB edge motif to attain structural rigidity of edges, and importantly the maximum number of vertex crossovers between each duplex in adjacent edges to also endow overall rigidity and ideally planarity across the complete object (Fig. 1). While this multi-layer design with multiway vertex connections was previously shown to enhance in-plane structural integrity significantly compared with corresponding DX-based objects composed of only two duplexes per edge, AFM and TEM characterization in that work was unable to determine out-of-plane deformations versus planarity of the fabricated structures in solution³⁵.
 - Using distinct target boundary geometries including a hexagon and pentagon, we used cryo-EM to first evaluate planarity for these objects with and without an internal mesh (Fig. 2). The internal mesh was originally introduced to reinforce the in-plane structural fidelity of the target 2D wireframe structures, which were verified using AFM and TEM to have accurate target angles between neighboring arms³⁵. Cryo-EM imaging and 3D reconstruction here verified that the objects not only have accurate internal angles but also remain planar within ~6 nm across their lateral 80 nm dimension, irrespective of whether or not the internal mesh is present (Fig. 2). The hexagon and pentagon with internal mesh structures were assigned a minimum edge length of 84 bp, whereas their corresponding hollow structures were assigned a minimum edge length of 106 bp for the hexagon and 122 bp for the pentagon to achieve the same diameter of 80 nm. As shown in Fig. 2a, the hexagonal structure with internal mesh is in agreement with our design when facing up during imaging, which is consistent with its AFM and TEM images³⁵, although now the structures were frozen in solution without any surface-imposed restrictions.
 - Individual DNA structures in different orientations are also identifiable in vitreous ice, with their planarity apparent from different orientations of the 2D objects, and the most apparent case evident from 2D objects in a vertical orientation (Fig. S2). Similar observations were made for the pentagonal structure with internal mesh (Fig. S3), as well as for the hexagonal and pentagonal

Science Advances Manuscript Template Page 3 of 18

structures without internal mesh. As shown in Fig. S4-S5, both the hollow hexagon and pentagon 139

- are planar in solution, appearing as a straight line when oriented vertically in cryo-EM imaging.
- While the preponderance of objects appeared planar at the single-particle level, occasionally 141
- structures also show some curvature (Fig. S2-S6). However, single-particle heterogeneity is 142
- sufficiently low that 2D class averages are easily generated (Fig. 1b and Fig. S3-S5). 143

Aside from achieving planarity for complex wireframe origami objects, these 3D reconstructions 144

- also offer the first reported examples of 2D cryo-EM DNA origami structures with a size of 80 nm
- that we are aware of. Rotation of the objects along one axis reveals not only planarity but also lack 146
 - of overall twist, observed in another study¹². Interestingly, while most of the 6HB edges in our
- structures do not show significant twist, the internal mesh of the pentagonal object does exhibit a 148
- left-handed twist that is apparent on the inner, spoke edges. This is consistent with the correlation 149
- coefficient between the pseudo-atomic model and density map: the pentagonal structure with 150
- internal mesh has a correlation coefficient of 0.75, which is lower than hexagonal structure with 151
- internal mesh (0.82). For the hollow hexagon and pentagon, the correlation coefficients are 0.84 152
- and 0.83, respectively (Table S2). Resolutions of the four objects are also comparable, with the 153
- hexagon and pentagon with internal mesh reconstructed to a resolution of 18 Å and 17 Å, 154
- respectively, and the two hollow structures reconstructed to 16 Å resolution. 155

Impact of edge length on planarity

140

145

147

156

157

158

159

160

161

163

181

pentagon as a model geometry to investigate whether changing edge length may impact planarity. Comparison of 84 bp and 122 bp minimum edge length pentagonal structures showed retention of planarity despite significant changes in edge-length, with resolutions of 16 Å based on FSC curves

In light of the planarity achieved by wireframe origami without an internal mesh, we chose the

- (Fig. 3a and Fig. S5-S6). For both structures, the pseudo-atomic model prediction (PDB file) generated by ATHENA fits well within the density map, with the same correlation coefficient of 162
 - 0.83, and there is no obvious twisting along the edges regardless of the differing edge lengths.
- Because the differences in edge lengths between the two structures is not an integer number of 164
- helical turns of DNA, the staple crossover patterns in the vertices are different between the two 165
- pentagons even though the vertex angles are the same for both objects (Fig. S7). The fact that the 166
- resolution, model fitting, and quality of both cryo-EM structures are the same suggests that our 167
- vertex design parameters are likely to be generally valid. A discrete advantage of using a 6HB edge 168
- compared with a single DNA-duplex- or DX-based edge is its relatively large persistence length of 169 1-2 µm associated with its rigidity^{41,42}, which is essential for the structural integrity of wireframe 170
- DNA origami, particularly for the hollow structures fabricated here. To further investigate edge-171
- length variation, five pentagonal structures with edge lengths ranging from 42 bp to 210 bp (14 to 172
- 71 nm) were characterized by cryo-EM imaging (Fig. 3b). Smaller sized pentagons of 42 bp to 126 173
- bp edge lengths can readily adapt to different orientations in vitreous ice, with their planarity 174
- observed in cryo-EM imaging. In contrast, pentagons with 168 bp edge length appeared largely 175 regular, although they adopted fewer distinct orientations during imaging due to their larger size 176
- (~100 nm diameter). When the edge length reached 210 bp, kinking and bending was observable 177
- 178 along the edge and vertex of the pentagonal structure, suggesting an upper limit of ~100 nm overall
- dimension and ~60 nm edge-length for METIS to realize planar objects with accurate internal target 179
- angles based on cryo-EM imaging results (Fig. 3b). 180

Rendering symmetric versus asymmetric objects

To test whether planarity is retained with asymmetric objects, asymmetric and symmetric triangles 182 with equal maximum edge lengths of 84 bp were examined, with reconstruction global resolutions 183

of 11 Å and 13 Å, respectively, and planarity again retained together with target internal angles (Fig. 4 and Fig. S8-S9). To investigate the structural fidelity of the triangular structures, pseudoatomic models generated by ATHENA were used to fit the density maps from the 3D cryo-EM reconstructions. The total correlation coefficient between the atomic model and density map was 0.85 for the symmetric triangle, and 0.87 for the asymmetric triangle. For the symmetric triangle, there was missing density in the vertex, as can be seen from the reconstructed density map. This is consistent with molecular dynamics simulations performed in previous work³⁵, in which higher local conformational flexibilities at the vertices were observed. The local resolution maps also show lower resolutions of both symmetric and asymmetric triangle in all the vertices, whereas the highest resolutions are observed in the edge, with up to 10 Å for symmetric triangle (Fig. S10). For the asymmetric triangle, although the vertices show better resolved electron density, the shortest edge exhibits outward bowing that is only slightly visible in the other edges of this and the symmetric triangular object. Comparison of the cryo-EM reconstruction of symmetric and asymmetric triangles also offered the ability to test whether the resolution of the symmetric structures is limited by imposing symmetry during class-averaging and 3D reconstruction. Fig. S11 shows the linear correlation between particle number and map resolution⁴³, with B-factors estimated to be 1954.5 $Å^2$ and 2276.8 $Å^2$ for the symmetric and asymmetric triangle, respectively. Because it can be inferred from these plots that using the same number of particles (or even triple the number) for reconstruction will result in similar resolutions for the symmetric and asymmetric triangles, this suggests that the limitation in resolution does not only arise from symmetry, but vertex design and overall 6HB rigidity and structural fidelity are likely also factors that limit the highest resolution that can be achieved. With an 11 Å global resolution for symmetric triangles and 13 Å for asymmetric triangles, these represent the highest resolutions achieved for 6HB structures to date.

Molecular simulation of 2D origami objects

To gain dynamical insight into the molecular-level structure and flexibility of the designed origami objects, we performed coarse-grained molecular dynamics simulations with oxDNA2 to complement experimental cryo-EM data (Fig. 5). The oxDNA2 coarse-grained model was used because it accurately represents the thermodynamic and mechanical properties of DNA while enabling long time-scale simulations at lower computational cost compared with classical all-atom models^{44,45}. As the largest and most complex wireframe origami folded in this study, the hexagonal and pentagonal DNA origami objects with internal meshes were first chosen for oxDNA2 simulation (Fig. S12, S13). Simulations demonstrated general planarity of 2D DNA objects and varied flexibility for different objects, indicated by values of RMSF (Root Mean Square Fluctuations) relative to the mean structure (Fig. 5). Compared with the hexagon, the pentagonal structure exhibited higher flexibility in vertices, consistent with our experimental data that showed missing density and curved edges in the reconstructed pentagonal object. In addition, the two triangles with the highest structural resolutions were simulated, with the symmetric triangle in good agreement with our previous fully atomistic MD simulation³⁵. Moreover, there are lower RMSF values of both triangular objects compared to larger structures such as the hexagon and pentagon. However, the RMSF analysis reveals a higher flexibility at the vertices, while the edges showed only minor temporary deviations from planarity leading to very flat structures on average (detailed RMSF values and structure files are provided as Supplementary Information). At the level of individual helices, the greater spacing between crossovers and loops led to a larger flexibility at the vertices compared to the edges, and more pronounced splaying at the inside of sharp bends. Taken together, these simulations corroborate the high structural fidelity and planarity of these METISdesigned 2D DNA origami objects observed using cryo-EM.

Discussion

184

185

186

187

188

189

190 191

192

193 194

195

196 197

198

199

200

201

202

203

204

205

206

207

208

209

210211

212

213

214

215

216

217

218

219

220

221

222

223224

225

226

227

228

229230

232
233
2D DN
234
with app
235
others.
236
using th
237
regular
238
internal
239
asymme
240
10 Å re
241
origami
242
the ME
243
althoug
244
origami

245

246

247

248

249

250251252

253

254

255

256257

258259

260

261

262

263

264

265

266

267

268

269

270

271

272273

274

275

276

277

278279

280

2D DNA origami is emerging as a very widely used template for functional materials fabrication, with applications to molecular biophysics²³, excitonics¹⁵⁻¹⁸, photonics²⁴, and plasmonics¹⁴, amongst others. In the present work, we investigate the planarity of 2D wireframe DNA origami designed using the algorithm METIS, as characterized by free standing cryo-EM. Planarity was exhibited by regular shapes such as hexagonal and pentagonal objects, whether reinforced internally with an internal mesh or not, up to an overall lateral dimension of ~80 nm. In addition, an irregular, asymmetric triangle was reconstructed to 13 Å resolution by cryo-EM, which, together with up to 10 Å resolution for the symmetric triangle, represent the highest resolutions to date for DNA origami cryo-EM structures based on the 6HB motif. The enhanced vertex designs employed by the METIS algorithm suggest that diverse classes of 2D objects designed will remain planar. although further experimentation is needed to support this hypothesis. These 2D planar DNA origami may be employed in the future as a platform for the judicious placement of functional components, such as proteins^{28,46,47}, chromophores^{48,49}, and nanoparticles^{50,51} with high structural fidelity in solution, which opens exciting possibilities for diverse 2D functional materials and biomolecular applications accessible to a broad community of researchers through the open source software METIS and its GUI ATHENA.

Materials and Methods

Top-down sequence design

ATHENA was used to design 2D DNA wireframe structures using the METIS "top-down" approach. It is provided online for use as standalone open-source software (https://github.com/lcbb/athena) for the custom design of 2D & 3D wireframe scaffolded DNA origami objects. Output files include staple strand sequences (Tables S3-S14) and PDB files for oxDNA simulations to study structural and conformational dynamics.

Materials

DNA origami staple strands were purchased in 96-well plate format from Integrated DNA Technologies, Inc. at 25-nmole synthesis scale, with strands purified by standard desalting and calibrated to 200 μM based on full yield. Staple strands were mixed in equal volume from the corresponding wells and used directly for DNA origami folding without further purification. DNA scaffolds of lengths 2,775- and 7,249-nt were used. The 2,775-nt DNA scaffold was produced using restriction enzyme cloning. The 2,775-nt plasmid assembled using restriction enzyme cloning was transformed into *E. coli* containing the M13cp helper plasmid. The 2,775 nt scaffold was subsequently amplified in bacteria in 2xYT incubated for 8 hours at 37°C, then harvested and purified⁵². The 7,249 nt DNA scaffold (M13mp18) was purchased from Guild BioSciences at a concentration of 100 nM. 10x TAE buffer was purchased from Alfa Aesar. Magnesium acetate tetrahydrate (molecular biology grade) was purchase from MilliporeSigma. 1x TAE buffer with 12.5 mM Mg(OAc)₂ was prepared with 10x TAE buffer and magnesium acetate tetrahydrate. Agarose (molecular biology grade) was purchased from IBI Scientific.

Origami self-assembly

All METIS structures were folded following the same protocol. 10 nM of DNA scaffold was mixed with 15 equiv corresponding staples strands in 1x TAE buffer with 12.5 mM Mg(OAc)₂, the final volume of the self-assembly solution was 100 μ L. The mixture buffer solution was annealed in a PCR thermocycler: 95 °C for 2 min, 80 °C to 20 °C at a rate of 0.5 °C per 10 min. The annealed solution was diluted into 300 μ L with 1x TAE buffer with 12.5 mM Mg(OAc)₂, and the extra staple strands were removed with MWCO = 100 kDa spin filter concentration columns. The purified DNA

Science Advances Manuscript Template Page 6 of 18

origami solution was concentrated in the meantime and adjusted to desired concentrations (300 nM) for cryo-EM imaging.

Cryo-EM Imaging and 3D reconstruction

281

282 283

284

285

286

287288

289

290

291

292

293

294

295

296

297

298

299

300

301

302

303

304

305

306

307

308

309

310

311

312313

314

315

316

317

318

319

320

321

322

323

324

325

326

327

328329

330

For cryo-EM imaging only: The purified and concentrated DNA origami samples (3 µL) were applied to glow-discharged copper C-flat thick R2/1 300-mesh grids and frozen in liquid ethane using a Vitrobot (ThermoFisher) with 3 s blot. Grids were then imaged on a Talos Arctica scope (ThermoFisher) with a Falcon 3EC detector, operated at 200 kV and 57,000x magnification (2.54) Å nominal pixel size), using EPU software (ThermoFisher) to collect micrographs. For the cryo-EM imaging and 3D reconstructions: Three microliters of the DNA origami samples were applied onto the glow-discharged 200-mesh Quantifoil 2/1 grid coated with continuous carbon film, blotted for 2 s and rapidly frozen in liquid ethane using a Vitrobot Mark IV (Thermo Fisher Scientific). For hexagonal DNA origami with internal mesh (84 bp edge-length), pentagonal DNA origami with internal mesh (84 bp edge-length), and pentagonal DNA origami without internal mesh (84 bp edgelength), the grids were imaged on a Titan Krios G3i cryo-electron microscope (Thermo Fisher Scientific) operated at 300 kV at a magnification of 53,000× (corresponding to a calibrated sampling of 1.7 Å per pixel). Micrographs were recorded by EPU software (Thermo Fisher Scientific) with a Gatan K3 direct electron detector in counting mode, where each image is composed of 30 individual frames with an exposure time of 6 s and a total dose of ~40 electrons per Å². A total of 1594 images for the hexagonal DNA origami with internal mesh (84 bp edgelength), 1048 images for the pentagonal DNA origami with internal mesh (84 bp edge-length), and 1100 images for the pentagonal DNA origami without internal mesh (84 bp edge-length) were collected with a defocus range of -1 - -3 µm. For hexagonal DNA origami without internal mesh (106 bp edge-length) and pentagonal DNA origami without internal mesh (122 bp edge-length), the grids were imaged on a Titan Krios G3i cryo-electron microscope (Thermo Fisher Scientific) operated at 300 kV at a magnification of 37,000× (corresponding to a calibrated sampling of 2.1 Å per pixel). Micrographs were recorded by EPU software (Thermo Fisher Scientific) with a Falcon 4 direct electron detector in gain-normalized mrc mode, where each image is composed of 20 individual frames with an exposure time of 10 s and a total dose of \sim 20 electrons per Å². A total of 1170 images for the hexagonal DNA origami without internal mesh (106 bp edge-length) and a total of 1331 images for the pentagonal DNA origami without internal mesh (122 bp edge-length) were collected with a defocus range of -2 - -3.5 um. For symmetric triangular DNA origami (84 bp edge-length) and asymmetric triangular DNA origami (84-73-63 bp edge-lengths), the grids were imaged on a Talos Arctica G2 cryo-electron microscope (Thermo Fisher Scientific) operated at 200 kV at a magnification of 64,000× (corresponding to a calibrated sampling of 1.4 Å per pixel). Micrographs were recorded by EPU software (Thermo Fisher Scientific) with a Gatan K3 direct electron detector in counting mode, where each image is composed of 40 individual frames with an exposure time of 2.5 s and a total dose of ~50 electrons per Å². A total of 4093 images for the symmetric triangular DNA origami (84 bp edge-length) and a total of 4135 images for the asymmetric triangular DNA origami (84-73-63 bp edge-lengths) were collected with a defocus range of $-1.5 - -3.5 \mu m$.

Single-particle image processing and 3D reconstruction was performed as previously described⁵³. Briefly, all the images were motion-corrected using MotionCor2⁴⁹ and CTF was determined using CTFFIND4⁵⁰. All particles were autopicked using NeuralNet option in EMAN2⁵¹ and further checked manually, yielding 14,029 particles for hexagonal DNA origami with internal mesh (84 bp edge-length), 30,279 particles for pentagonal DNA origami without internal mesh (84 bp edge-length), 25,932 particles for pentagonal DNA origami without internal mesh (84 bp edge-length), 55,991 particles for pentagonal DNA origami without internal mesh (106 bp edge-length), 358,740 particles for symmetric triangular DNA origami (84 bp edge-length) and 304,395 particles for asymmetric

triangular DNA origami (84-73-63 bp edge-lengths). The particle coordinates were then imported to RELION⁵⁴, where 2D classification were performed to remove poor 2D class averages. For all objects, a variety of orientations of the particles and their 2D class averages were observed, including classes that were not perpendicular to the camera, which was important for 3D reconstruction. The final 3D refinements were performed in CryoSPARC⁵⁵ using 7,857 particles for hexagonal DNA origami with internal mesh (84 bp edge-length), 11,758 particles for pentagonal DNA origami with internal mesh (84 bp edge-length), 6,145 particles for pentagonal DNA origami without internal mesh (84 bp edge-length), 21,809 particles hexagonal DNA origami without internal mesh (106 bp edge-length), 28,628 particles for pentagonal DNA origami without internal mesh (122 bp edge-length), 263,617 particles for symmetric triangular DNA origami (84 bp edgelength) and 95,277 particles for asymmetric triangular DNA origami (84-73-63 bp edge-lengths); the corresponding maps were achieved with resolutions of 18 Å, 17 Å, 16 Å, 16 Å, 16 Å, 11 Å and 13 Å, respectively, based on the FSC of two independent particle data sets at a threshold of 0.143. Figures were prepared using Chimera. Notably, the 3D refinements were performed with and without symmetry applied for the symmetric objects. While the resulting maps with and without symmetry were similar, the resolution and correlation coefficient are generally lower without symmetry, and we chose to highlight those with symmetry which would have a better statistically defined map compared with the models. The resolutions described in this study were all based on reconstructions assuming symmetry.

Coarse-grained molecular dynamics simulations using oxDNA2 model

MD simulations of DNA nanostructures were performed using the oxDNA2 model and simulation software 44,45,56,57. The oxDNA model is a coarse-grained approximation to study the thermodynamic and mechanical properties of DNA, enabling longer time scales and larger system sizes to be simulated 44,45. Fully atomistic DNA nanostructures from ATHENA were converted into oxDNA file format using tacoxDNA58. Systems were simulated at a salt concentration of 1 M [Na⁺], as recommended by the developers of oxDNA to represent typical experimental conditions.³ All structures were energy minimized for 2000 steps, followed by short simulations to equilibrate the structures for 3.03-30.3 μs (10⁶-10⁷ steps) at 300 K using the Langevin thermostat (diff_coeff 2.5). The production simulations were run for 0.303 ms (10⁸ steps, time step: 0.1515 ps) at 300 K using the Anderson-like john thermostat (diff_coeff 2.5). Initial velocities were refreshed from a Maxwellian distribution. The simulations were visualized using oxView and analyzed using oxDNA analysis tools^{57,59}.

References

331

332

333

334

335

336

337338

339

340

341

342

343344

345

346

347

348

349

350

351

352

353

354

355

356

357

358

359

360

361

362363364

365

366

367

368

369

370

371372

373

374

375

376377

378379

- P. W. K. Rothemund, Folding DNA to create nanoscale shapes and patterns. *Nature* **440**, 297-302 (2006).
- S. M. Douglas, A. H. Marblestone, S. Teerapittayanon, A. Vazquez, G. M. Church, W. M. Shih, Rapid prototyping of 3D DNA-origami shapes with caDNAno. *Nucleic Acids Res.* **37**, 5001-5006 (2009).
- 3 C. E. Castro, F. Kilchherr, D.-N. Kim, E. L. Shiao, T. Wauer, P. Wortmann, M. Bathe, H. Dietz, A primer to scaffolded DNA origami. *Nat. Methods* **8**, 221-229 (2011).
- B. E. K. Snodin, J. S. Schreck, F. Romano, A. A. Louis, J. P. K. Doye, Coarse-grained modelling of the structural properties of DNA origami. *Nucleic Acids Res.* 47, 1585-1597 (2019).
- J. Yoo, A. Aksimentiev, In situ structure and dynamics of DNA origami determined through molecular dynamics simulations. *Proc. Natl. Acad. Sci.* **110**, 20099-20104 (2013).
- D.-N. Kim, F. Kilchherr, H. Dietz, M. Bathe, Quantitative prediction of 3D solution shape and flexibility of nucleic acid nanostructures. *Nucleic Acids Res.* **40**, 2862-2868 (2011).
- Z. Li, L. Wang, H. Yan, Y. Liu, Effect of DNA Hairpin Loops on the Twist of Planar DNA Origami Tiles. *Langmuir* **28**, 1959-1965 (2012).

Science Advances Manuscript Template Page 8 of 18

- H. Chen, T.-W. Weng, M. M. Riccitelli, Y. Cui, J. Irudayaraj, J. H. Choi, Understanding the Mechanical Properties of DNA Origami Tiles and Controlling the Kinetics of Their Folding and Unfolding Reconfiguration. *J. Am. Chem. Soc.* **136**, 6995-7005 (2014).
- R. Li, H. Chen, H. Lee, J. H. Choi, Elucidating the Mechanical Energy for Cyclization of a DNA Origami Tile. *Appl.* **11**, 2357 (2021).
- M. A. B. Baker, A. J. Tuckwell, J. F. Berengut, J. Bath, F. Benn, A. P. Duff, A. E. Whitten, K. E. Dunn, R. M. Hynson, A. J. Turberfield, L. K. Lee, Dimensions and Global Twist of Single-Layer DNA Origami Measured by Small-Angle X-ray Scattering. *ACS Nano* 12, 5791-5799 (2018).

393

396

397

398

402

403

407

408

- H. Chen, H. Zhang, J. Pan, T.-G. Cha, S. Li, J. Andréasson, J. H. Choi, Dynamic and Progressive Control of DNA Origami Conformation by Modulating DNA Helicity with Chemical Adducts. *ACS Nano* **10**, 4989-4996 (2016).
 - M. Kube, F. Kohler, E. Feigl, B. Nagel-Yüksel, E. M. Willner, J. J. Funke, T. Gerling, P. Stömmer, M. N. Honemann, T. G. Martin, S. H. W. Scheres, H. Dietz, Revealing the structures of megadalton-scale DNA complexes with nucleotide resolution. *Nat. Commun.* 11, 6229 (2020).
- 394 13 Z. G. Wang, Q. Liu, B. Q. Ding, Shape-Controlled Nanofabrication of Conducting Polymer on Planar DNA Templates. *Chem. Mater.* **26**, 3364-3367 (2014).
 - A. Kuzyk, R. Schreiber, Z. Fan, G. Pardatscher, E.-M. Roller, A. Högele, F. C. Simmel, A. O. Govorov, T. Liedl, DNA-based self-assembly of chiral plasmonic nanostructures with tailored optical response. *Nature* **483**, 311-314 (2012).
- 599 15 E. A. Hemmig, C. Creatore, B. Wünsch, L. Hecker, P. Mair, M. A. Parker, S. Emmott, P. Tinnefeld, U. F. Keyser, A. W. Chin, Programming Light-Harvesting Efficiency Using DNA Origami. *Nano Lett.* 16, 2369-2374 (2016).
 - L. Olejko, I. Bald, FRET efficiency and antenna effect in multi-color DNA origami-based light harvesting systems. *RSC Adv.* 7, 23924-23934 (2017).
- M. Madsen, M. R. Bakke, D. A. Gudnason, A. F. Sandahl, R. A. Hansen, J. B. Knudsen, A. L. B.
 Kodal, V. Birkedal, K. V. Gothelf, A Single Molecule Polyphenylene-Vinylene Photonic Wire. ACS
 Nano. 15, 9404–9411 (2021).
 - 18 X. Wang, C. Li, D. Niu, R. Sha, N. C. Seeman, J. W. Canary, Construction of a DNA Origami Based Molecular Electro-optical Modulator. *Nano Lett.* **18**, 2112-2115 (2018).
- M. Endo, H. Sugiyama, Single-Molecule Imaging of Dynamic Motions of Biomolecules in DNA Origami Nanostructures Using High-Speed Atomic Force Microscopy. *Acc. Chem. Res.* **47**, 1645-1653 (2014).
- N. V. Voigt, T. Tørring, A. Rotaru, M. F. Jacobsen, J. B. Ravnsbæk, R. Subramani, W. Mamdouh, J. Kjems, A. Mokhir, F. Besenbacher, K. V. Gothelf, Single-molecule chemical reactions on DNA origami. *Nat. Nanotechnol.* **5**, 200-203 (2010).
- J. B. Knudsen, L. Liu, A. L. B. Kodal, M. Madsen, Q. Li, J. Song, J. B. Woehrstein, S. F. J. Wickham, M. T. Strauss, F. Schueder, J. Vinther, A. Krissanaprasit, D. Gudnason, A. A. A. Smith, R. Ogaki, A. N. Zelikin, F. Besenbacher, V. Birkedal, P. Yin, W. M. Shih, R. Jungmann, M. D. Dong, K. V. Gothelf, Routing of individual polymers in designed patterns. *Nat. Nanotechnol.* **10**, 892-898 (2015).
- R. Jungmann, M. S. Avendaño, J. B. Woehrstein, M. Dai, W. M. Shih, P. Yin, Multiplexed 3D cellular super-resolution imaging with DNA-PAINT and Exchange-PAINT. *Nat. Methods* 11, 313-318 (2014).
- W. Engelen, H. Dietz, Advancing Biophysics Using DNA Origami. *Annu. Rev. Biophys.* **50**, 469-424 (2021).
- E.-C. Wamhoff, J. L. Banal, W. P. Bricker, T. R. Shepherd, M. F. Parsons, R. Veneziano, M. B. Stone, H. Jun, X. Wang, M. Bathe, Programming Structured DNA Assemblies to Probe Biophysical Processes. *Annu. Rev. Biophys.* **48**, 395-419 (2019).
- 428 25 Q. Zhang, Q. Jiang, N. Li, L. Dai, Q. Liu, L. Song, J. Wang, Y. Li, J. Tian, B. Ding, Y. Du, DNA 429 Origami as an In Vivo Drug Delivery Vehicle for Cancer Therapy. *ACS Nano* **8**, 6633-6643 (2014).
- M. Bathe, L. A. Chrisey, D. J. C. Herr, Q. Lin, D. Rasic, A. T. Woolley, R. M. Zadegan, V. V. Zhirnov, Roadmap on biological pathways for electronic nanofabrication and materials. *Nano Futures* 3, 012001 (2019).

Science Advances Manuscript Template Page 9 of 18

- Q. Jiang, C. Song, J. Nangreave, X. Liu, L. Lin, D. Qiu, Z.-G. Wang, G. Zou, X. Liang, H. Yan, B. Ding, DNA Origami as a Carrier for Circumvention of Drug Resistance. *J. Am. Chem. Soc.* **134**, 13396-13403 (2012).
- 436 28 R. Veneziano, T. J. Moyer, M. B. Stone, E.-C. Wamhoff, B. J. Read, S. Mukherjee, T. R. Shepherd, J. Das, W. R. Schief, D. J. Irvine, M. Bathe, Role of nanoscale antigen organization on B-cell activation probed using DNA origami. *Nat. Nanotechnol.* **15**, 716-723 (2020).

442

443

444

445

446 447

448

449

450

451 452

453

454

455

459

460

461

462

463

464 465

469

470

471

472

- 439 29 A. Gopinath, P. W. K. Rothemund, Optimized Assembly and Covalent Coupling of Single-Molecule DNA Origami Nanoarrays. *ACS Nano* **8**, 12030-12040 (2014).
 - A. Gopinath, E. Miyazono, A. Faraon, P. W. K. Rothemund, Engineering and mapping nanocavity emission via precision placement of DNA origami. *Nature* **535**, 401-405 (2016).
 - K. F. Wagenbauer, C. Sigl, H. Dietz, Gigadalton-scale shape-programmable DNA assemblies. *Nature* **552**, 78-83 (2017).
 - P. Wang, S. Gaitanaros, S. Lee, M. Bathe, W. M. Shih, Y. Ke, Programming Self-Assembly of DNA Origami Honeycomb Two-Dimensional Lattices and Plasmonic Metamaterials. *J. Am. Chem. Soc.* **138**, 7733-7740 (2016).
 - H. Dietz, S. M. Douglas, W. M. Shih, Folding DNA into Twisted and Curved Nanoscale Shapes. *Science* **325**, 725-730 (2009).
 - S. M. Douglas, H. Dietz, T. Liedl, B. Högberg, F. Graf, W. M. Shih, Self-assembly of DNA into nanoscale three-dimensional shapes. *Nature* **459**, 414-418 (2009).
 - H. Jun, X. Wang, W. P. Bricker, M. Bathe, Automated sequence design of 2D wireframe DNA origami with honeycomb edges. *Nat. Commun.* **10**, 5419 (2019).
 - H. Jun, F. Zhang, T. Shepherd, S. Ratanalert, X. Qi, H. Yan, M. Bathe, Autonomously designed free-form 2D DNA origami. *Sci. Adv.* **5**, eaav0655 (2019).
- 456 37 É. Boulais, N. P. D. Sawaya, R. Veneziano, A. Andreoni, J. L. Banal, T. Kondo, S. Mandal, S. Lin, G. S. Schlau-Cohen, N. W. Woodbury, H. Yan, A. Aspuru-Guzik, M. Bathe, Programmed coherent coupling in a synthetic DNA-based excitonic circuit. *Nat. Mater.* 17, 159-166 (2018).
 - J. L. Banal, T. Kondo, R. Veneziano, M. Bathe, G. S. Schlau-Cohen, Photophysics of J-Aggregate-Mediated Energy Transfer on DNA. *J. Phys. Chem. Lett.* **8**, 5827-5833 (2017).
 - J. K. Hannestad, P. Sandin, B. Albinsson, Self-Assembled DNA Photonic Wire for Long-Range Energy Transfer. *J. Am. Chem. Soc.* **130**, 15889-15895 (2008).
 - 40 H. Jun, X. Wang, Molly F. Parsons, William P. Bricker, T. John, S. Li, S. Jackson, W. Chiu, M. Bathe, Rapid prototyping of arbitrary 2D and 3D wireframe DNA origami. *Nucleic Acids Res.* **49**, 10265-10274 (2021).
- T. Wang, D. Schiffels, S. Martinez Cuesta, D. Kuchnir Fygenson, N. C. Seeman, Design and Characterization of 1D Nanotubes and 2D Periodic Arrays Self-Assembled from DNA Multi-Helix Bundles. *J. Am. Chem. Soc.* **134**, 1606-1616 (2012).
 - T. Liedl, B. Högberg, J. Tytell, D. E. Ingber, W. M. Shih, Self-assembly of three-dimensional prestressed tensegrity structures from DNA. *Nat. Nanotechnol.* **5**, 520-524 (2010).
 - P. B. Rosenthal, R. Henderson, Optimal Determination of Particle Orientation, Absolute Hand, and Contrast Loss in Single-particle Electron Cryomicroscopy. *J. Mol. Biol.* **333**, 721-745 (2003).
- 473 44 P. Šulc, F. Romano, T. E. Ouldridge, L. Rovigatti, J. P. K. Doye, A. A. Louis, Sequence-dependent thermodynamics of a coarse-grained DNA model. *Chem. Phys.* **137**, 135101 (2012).
- J. P. K. F. Doye, H.; Prešern, D.; Bohlin, J.; Rovigatti, L.; Romano, F.; Šulc, P.; Wong, C. K.; Louis, A. A.; Schreck, J. S.; Engel, M. C.; Matthies, M.; Benson, E.; Poppleton, E.; Snodin, B. E. K., The OxDNA Coarse-Grained Model as a Tool to Simulate DNA Origami. *arxiv*, (2020).
- 478 46 P. Zhang, X. Liu, P. Liu, F. Wang, H. Ariyama, T. Ando, J. Lin, L. Wang, J. Hu, B. Li, C. Fan, Capturing transient antibody conformations with DNA origami epitopes. *Nat. Commun.* 11, 3114 (2020).
- 481 47 P. S. Kwon, S. Ren, S.-J. Kwon, M. E. Kizer, L. Kuo, M. Xie, D. Zhu, F. Zhou, F. Zhang, D. Kim, K. Fraser, L. D. Kramer, N. C. Seeman, J. S. Dordick, R. J. Linhardt, J. Chao, X. Wang, Designer DNA architecture offers precise and multivalent spatial pattern-recognition for viral sensing and inhibition. *Nat. Chem.* 12, 26-35 (2020).
- 485 48 P. K. Dutta, R. Varghese, J. Nangreave, S. Lin, H. Yan, Y. Liu, DNA-Directed Artificial Light-486 Harvesting Antenna. *J. Am. Chem. Soc.* **133**, 11985-11993 (2011).

Science Advances Manuscript Template Page 10 of 18

- W. P. Klein, B. S. Rolczynski, S. M. Oliver, R. Zadegan, S. Buckhout-White, M. G. Ancona, P. D. Cunningham, J. S. Melinger, P. M. Vora, W. Kuang, I. L. Medintz, S. A. Díaz, DNA Origami Chromophore Scaffold Exploiting HomoFRET Energy Transport to Create Molecular Photonic Wires. *ACS Appl. Nano Mater.* 3, 3323-3336 (2020).
- C. Hartl, K. Frank, H. Amenitsch, S. Fischer, T. Liedl, B. Nickel, Position Accuracy of Gold Nanoparticles on DNA Origami Structures Studied with Small-Angle X-ray Scattering. *Nano Lett.* 18, 2609-2615 (2018).
 - W. Liu, M. Tagawa, H. L. Xin, T. Wang, H. Emamy, H. Li, K. G. Yager, F. W. Starr, A. V. Tkachenko, O. Gang, Diamond family of nanoparticle superlattices. *Science* **351**, 582-586 (2016).
 - T. R. Shepherd, R. R. Du, H. Huang, E.-C. Wamhoff, M. Bathe, Bioproduction of pure, kilobase-scale single-stranded DNA. *Sci. Rep.* **9**, 6121 (2019).
 - S. Guo, M. Vieweger, K. Zhang, H. Yin, H. Wang, X. Li, S. Li, S. Hu, A. Sparreboom, B. M. Evers, Y. Dong, W. Chiu, P. Guo, Ultra-thermostable RNA nanoparticles for solubilizing and high-yield loading of paclitaxel for breast cancer therapy. *Nat. Commun.* 11, 972 (2020).
 - 54 S. H. W. Scheres, RELION: Implementation of a Bayesian approach to cryo-EM structure determination. *J. Struct. Biol.* **180**, 519-530 (2012).
 - A. Punjani, J. L. Rubinstein, D. J. Fleet, M. A. Brubaker, cryoSPARC: algorithms for rapid unsupervised cryo-EM structure determination. *Nat. Methods* **14**, 290-296 (2017).
 - L. Rovigatti, P. Šulc, I. Z. Reguly, F. Romano, A comparison between parallelization approaches in molecular dynamics simulations on GPUs. *J. Comput. Chem.* **36**, 1-8 (2015).
 - E. Poppleton, R. Romero, A. Mallya, L. Rovigatti, P. Šulc, OxDNA.org: a public webserver for coarse-grained simulations of DNA and RNA nanostructures. *Nucleic Acids Res.* W491–W498 (2021).
 - A. Suma, E. Poppleton, M. Matthies, P. Šulc, F. Romano, A. A. Louis, J. P. K. Doye, C. Micheletti, L. Rovigatti, TacoxDNA: A user-friendly web server for simulations of complex DNA structures, from single strands to origami. *J. Comput. Chem.* **40**, 2586-2595 (2019).
 - E. Poppleton, J. Bohlin, M. Matthies, S. Sharma, F. Zhang, P. Šulc, Design, optimization and analysis of large DNA and RNA nanostructures through interactive visualization, editing and molecular simulation. *Nucleic Acids Res.* **48**, e72-e72 (2020).

Acknowledgments

We thank Edward Brignole for assisting cryo-EM imaging. Cryo-EM images are collected at MIT.nano on a Talos Arctica microscope, which was a gift from the Arnold and Mabel Beckman Foundation.

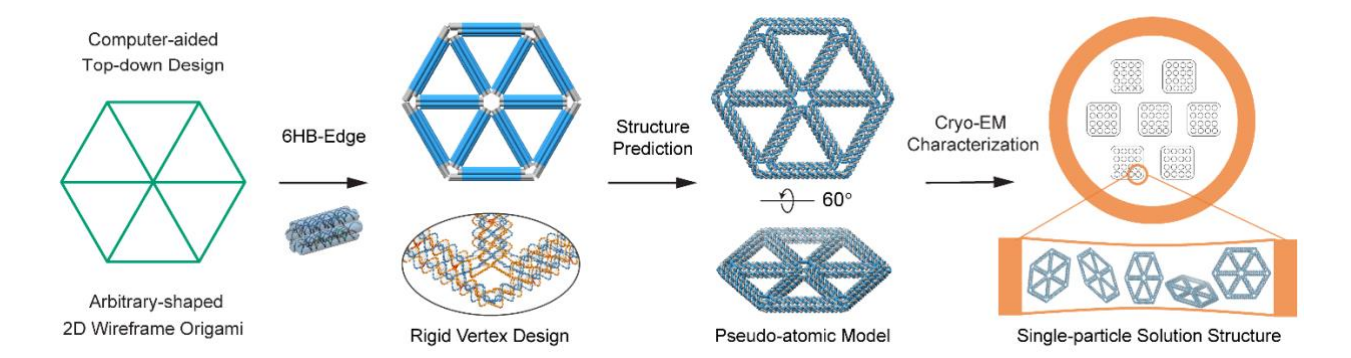
Funding: The authors are grateful for funding to the National Science Foundation NSF CBET-1729397 and CCF-1956054, the Office of Naval Research N00014-21-1-4013 and N00014-20-1-2084 (to W.C.), and the research was sponsored by the U.S. Army Research Office and accomplished under cooperative agreement W911NF-19-2-0026 for the Institute for Collaborative Biotechnologies (ICB Subaward KK1955). T.J. gratefully acknowledges financial support from the Alexander von Humboldt Foundation through a Feodor-Lynen Research Fellowship. H.F. is grateful to the EPSRC for support through the Centre for Doctoral Training Theory and Modelling in Chemical Sciences, under grant EP/L015722/1.

Author contributions: X.W., H.J. and M.B. conceived the research. X.W. implemented the origami design and experimental assay, collected, and analyzed the results to make the Figures. S.L. implemented the experimental assay, collected, and analyzed the experimental data. H.J. implemented the autonomous design algorithm and optimized Figures. K.Z. analyzed the experimental data. T.J., H.F. and J.D. implemented the theoretical analyses. X.W., S.L., T.J., and M.B. wrote the manuscript. M.B. supervised the project. All authors commented on and edited the manuscript.

Science Advances Manuscript Template Page 11 of 18

Competing interests: The authors declare they have no competing interests.

539540541542543544545



549550551552553554555

Fig. 1. Cryo-EM characterization of 2D wireframe structures. The input used for ATHENA software can be specified as arbitrary shaped target geometries. Based on the target geometry, the METIS algorithm was used to generate scaffold and staples routing of wireframe DNA origami with six-helix-bundle (6HB) edges. Maximum crossovers between adjacent edges are used to ensure the rigidity of the vertex design. The pseudo-atomic model was generated to compare to the structure determined by cryo-EM 3D reconstruction.

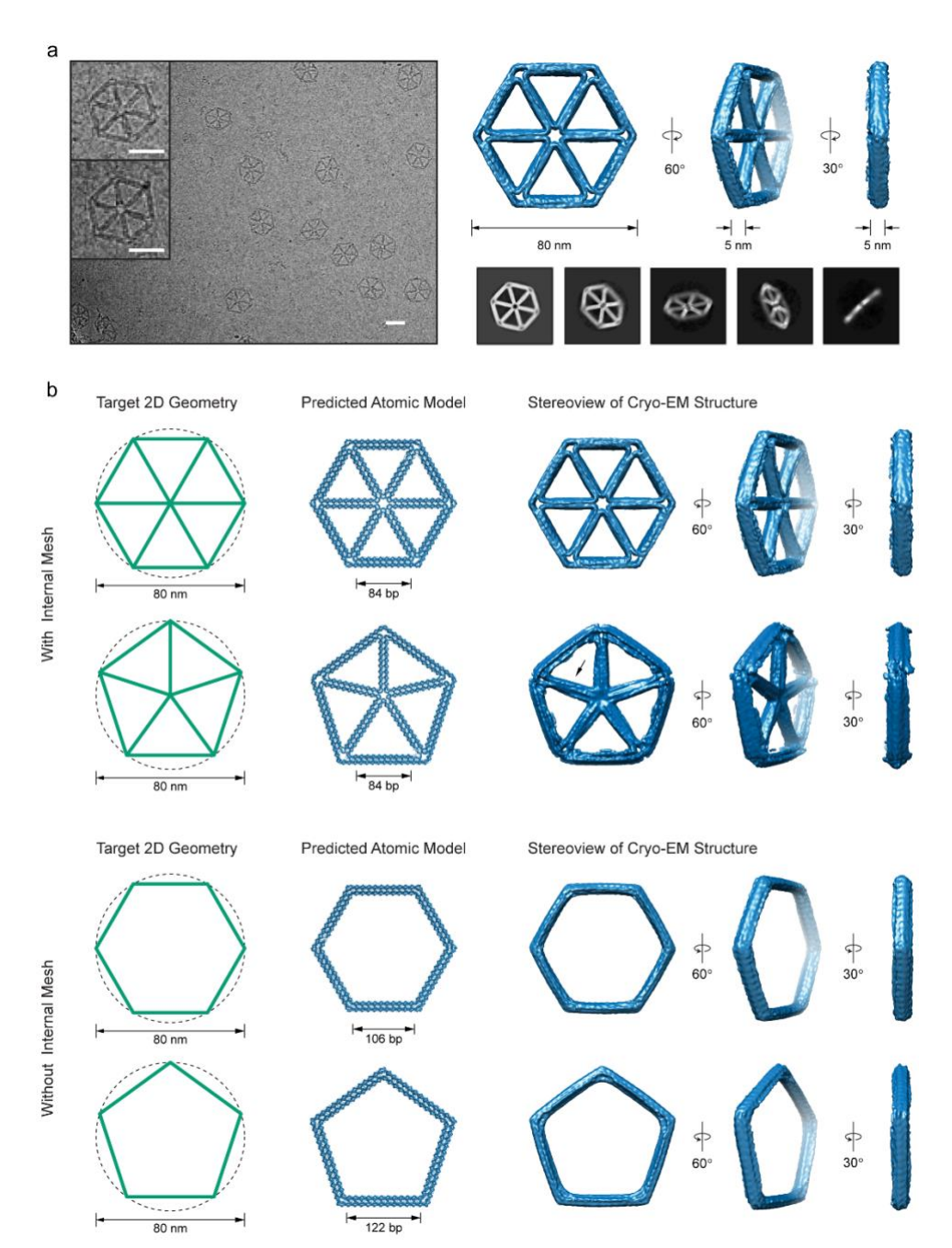
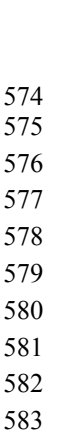


Fig. 2. 6HB-based wireframe DNA origami structures with and without internal mesh characterized by cryo-EM. (a) A representative METIS 2D wireframe DNA origami structure characterized by cryo-EM: a hexagonal origami with internal mesh. Different random orientations of the structure under cryo-EM imaging and 2D class-averages reflected its planarity. 3D reconstruction shows the hexagonal origami structure is 2D and planar, with a diameter of 80 nm and a thickness of only 5 nm. Scale bars: 50 nm. **(b)** Two different geometries (hexagon and pentagon) with the same diameter were generated with the computer-aided design tool. The predicted atomic models are compared to the reconstructed 3D structures, which show good matches for all four structures. As demonstrated by side views, the wireframe structures without internal mesh show almost perfect planarity, similar to the corresponding structures with internal mesh. No significant twisting was observed for most of the edges shown above, except the internal mesh edges of the pentagon structure as pointed out by the arrow (row 2). Missing density in the vertex was also observed in these areas.



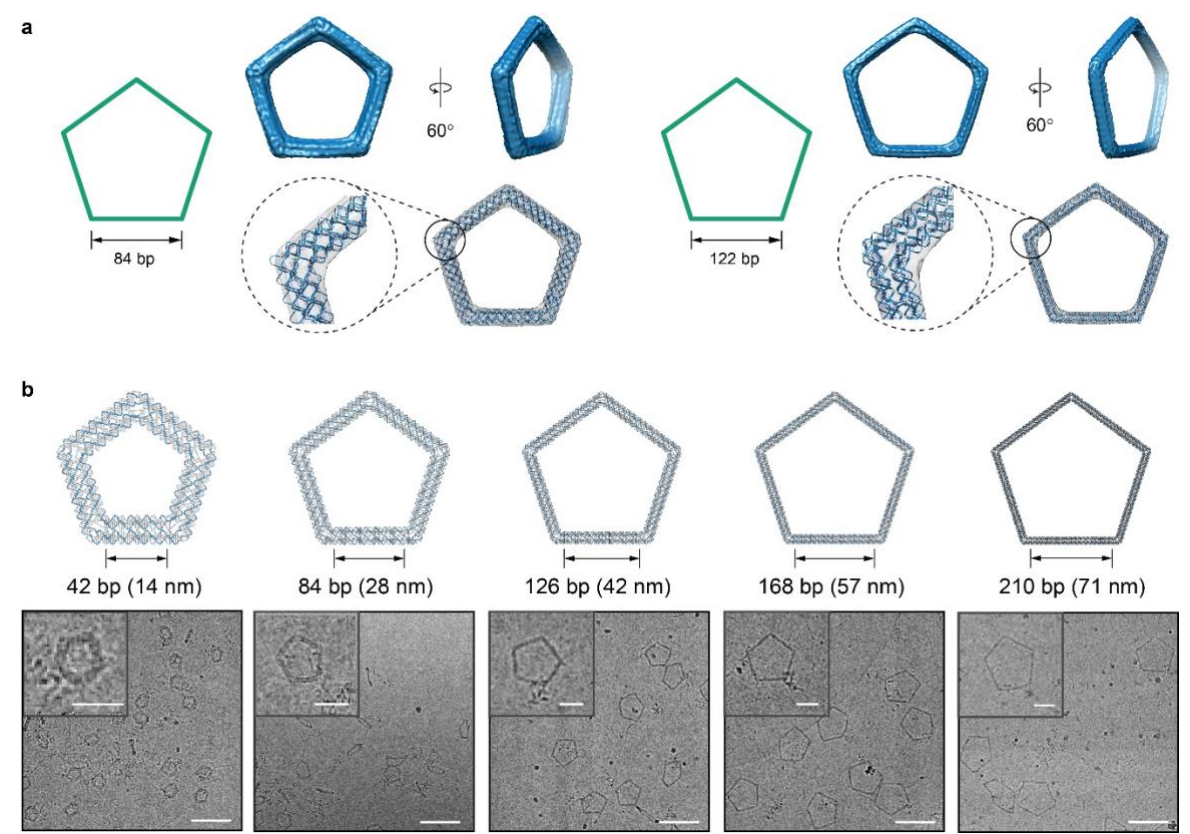


Fig. 3. Pentagon-shaped wireframe DNA origami structures designed with different edge lengths and characterized by cryo-EM. (a) The 3D reconstruction of two pentagon structures, one designed with 84 bp minimum edge length, the other designed with 122 bp minimum edge length. Both structures are planar and their vertex designs match well with the reconstructed structure. **(b)** Cryo-EM imaging of different sized pentagon structures, from 42 bp to 210 bp edge length. Scale bars: 50 nm and 100 nm (zoom-in and zoom-out images, respectively).

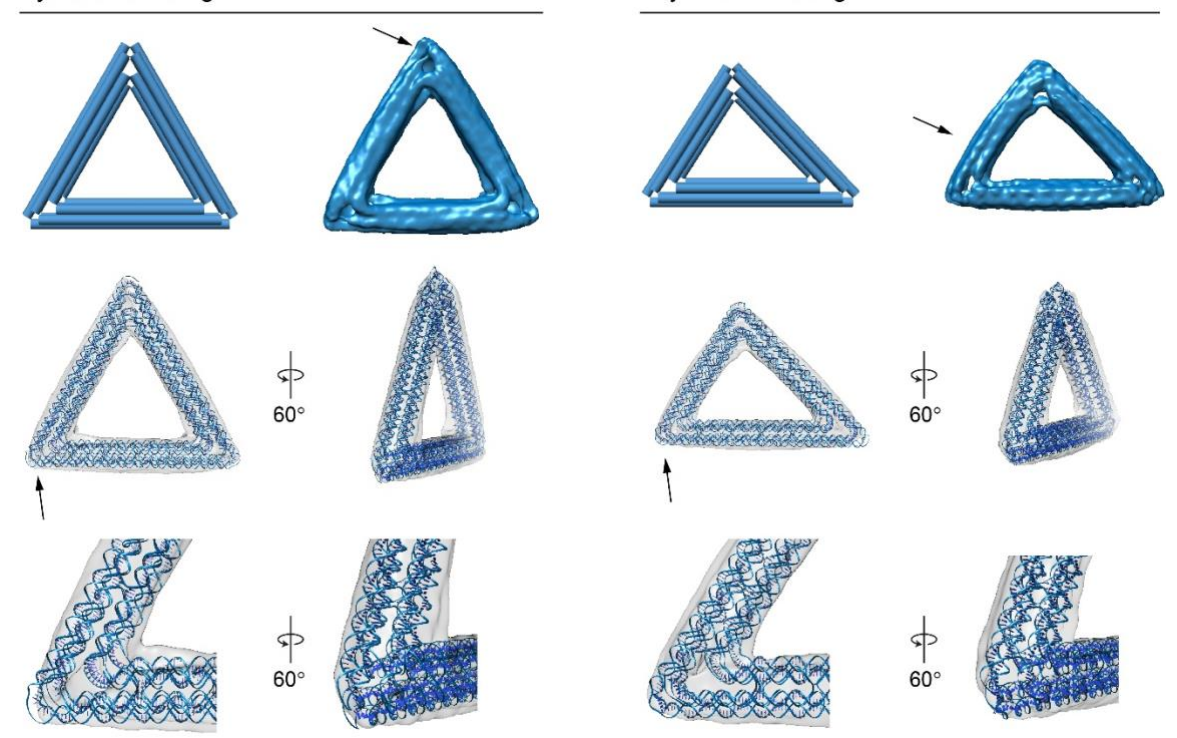


Fig. 4. Comparison between symmetric and asymmetric triangle structures. A symmetric triangle with equal edge lengths of 84 bp, and an asymmetric triangle with edge lengths of 84-73-63 bp were characterized by cryo-EM. The fitting between pseudo-atomic model and density map shows good agreement between the design and reconstructed structure. For both structures, the features that show disagreement were highlighted, such as the missing of density in the vertex for the symmetric triangle and the slight bowing of the edge for the asymmetric triangle.

Fig. 5. Comparison between oxDNA2 coarse-grained simulations and cryo-EM structures. Hexagonal and pentagonal origami with internal mesh, and symmetric and asymmetric triangles were chosen for oxDNA simulations. Subtle structural features predicted by the simulations are consistent with experimental observations, as highlighted by arrows. The structures from the trajectory with the lowest RMSF to the mean structure are shown (= centroid structures). The RMSF (nm) values were represented as a color bar: 0.64 (blue) to 4.84 (red). Ranges of RMSF (nm) for each structure, from top to bottom: 1.14-3.15; 1.43-4.84; 0.64-1.70; 0.67-1.92.

605	
606	Figs. S1 to S13
607	Tables S1 to S14
608	
609	The simulation results were provided as a separate Supplementary Materials file as a zip file,
610	which contains the results of ox-DNA simulations shown in main text Figure 5.
611	
612	oxDNA-results:
613	
614	Asymmetric_triangle_84bp (top file; centroid structure; mean structure; RMSF file)
615	Hexagon_mesh_84bp (top file; centroid structure; mean structure; RMSF file)
616	Pentagon_mesh_84bp (top file; centroid structure; mean structure; RMSF file)
617	Symmetric_triangle_84bp (top file; centroid structure; mean structure; RMSF file)
618	Readme-oxDNA-results
619	

Supplementary Materials